Jeong *et al.*
Cell Communication and Signaling (2025) 23:1
https://doi.org/10.1186/s12964-024-01996-x

Cell Communication and Signaling

RESEARCH

Open Access

Role of the Notch signaling pathway in porcine oocyte maturation

Pil-Soo Jeong[1†], Hyo-Gu Kang[1†], Dabin Cha[2], Se-Been Jeon[1], Min Ju Kim[1], Bong-Seok Song[1], Bo-Woong Sim[1,3*] and Sanghoon Lee[2*]

Abstract

Background Although the Notch signaling pathway is known to play an important role in ovarian follicle development in mammals, whether it is involved in oocyte maturation remains unclear. Therefore, this study was performed to elucidate the existence and role of the Notch signaling pathway during oocyte maturation in a porcine model.

Methods Reverse transcription-polymerase chain reaction (RT-PCR) and immunocytochemical assays were used to determine the existence of Notch signaling pathway-related transcripts and proteins in porcine cumulus–oocyte complexes (COCs). In vitro maturation (IVM) and parthenogenetic activation of oocytes were employed to examine the effects of Notch signaling inhibition on meiotic progression and embryogenesis of COCs using RO4929097 (RO), an inhibitor of γ secretase. Various staining methods (TUNEL, Phalloidin-TRITC, MitoTracker, JC-1, BODIPY FL ATP, ER-Tracker, Fluo-3, and Rhod-2) and immunocytochemical and quantitative PCR assays were used to identify the effects of Notch signaling inhibition on meiotic progression, embryogenesis, cell cycle progression, spindle assembly, chromosome alignment, mitochondrial and endoplasmic reticulum distribution, and downstream pathway targets in COCs.

Results The RT-PCR and immunocytochemical analyses revealed the presence of Notch signaling-related receptors (NOTCH1–4) and ligands (JAG1 and 2 and DLL1, 3, and 4) at 0, 22, 28, and 44 h of IVM in the COCs. RO treatment during oocyte maturation markedly reduced meiotic maturation and embryogenesis, inhibiting the cell cycle progression, spindle assembly, and chromosome alignment processes that are important for meiotic maturation. Furthermore, RO significantly impaired the cellular distribution and functions of the mitochondria and endoplasmic reticula, which are important organelles for the cytoplasmic maturation of oocytes. Finally, the involvement of canonical Notch signaling in oocyte maturation was confirmed by the decreased expression of HES and HEY family transcripts and proteins in the RO-treated COCs.

Conclusions It was first demonstrated that Notch signaling pathway-related transcripts and proteins were expressed during the meiotic maturation of porcine COCs. Furthermore, the inhibition of Notch signaling during IVM revealed the essential role of this signaling pathway during oocyte maturation in pigs.

Keywords Notch signaling pathway, γ secretase inhibitor, Oocyte maturation, Embryo development, Pig, Microtubule function, Organelle function

†Pil-Soo Jeong and Hyo-Gu Kang contributed equally to this work.

*Correspondence:
Bo-Woong Sim
embryont@kribb.re.kr
Sanghoon Lee
sanghoon@cnu.ac.kr
Full list of author information is available at the end of the article

Background

The ovary (the female gonad) is the only source of oocytes and important for the production of sex steroid hormones [1]. The ovarian follicles contain two types of cells: germ cells (oocytes) and somatic cells (granulosa and theca cells) [2]. During ovarian follicle development, the bidirectional communication between the oocyte and surrounding somatic cells regulate each other's proliferation and differentiation [3]. The interactions between these cells are highly coordinated by juxtracrine, autocrine, paracrine, and endocrine signals [3]. Although the molecular mechanism of ovarian follicle development is complex, several classical signaling pathways, including the Notch, Hedgehog, Wnt, and insulin pathways, have been reported to be involved [3]. Of these pathways, that of juxtacrine signaling has been the focus of research owing to the spatial relationships and interactions between the oocytes and surrounding somatic cells [4], with Notch being used the most, as it involves more direct cell-to-cell contact signaling [5].

The highly conserved Notch signaling pathway is involved in various biological processes, such as stem cell maintenance, adult tissue homeostasis, endothelial differentiation and fate determination, and tumor progression [6]. In mammals, five Notch ligands [Jagged (JAG) 1 and 2 and delta-like canonical Notch ligand (DLL) 1, 3, and 4] and four Notch receptors (NOTCH1–4) participate in the Notch signaling cascade [7]. As both Notch ligands and receptors are transmembrane proteins, the receptors are activated by their binding of ligands presented by neighboring cells [8]. Notch receptors undergo posttranslational modifications, including glycosylation and proteolysis (S1). When a ligand from one cell binds to a receptor on a neighboring cell, ligand endocytosis is triggered, exposing the metalloprotease recognition site on the receptor. S2 cleavage by ADAM10 leads to metalloprotease-mediated cleavage and removal of the extracellular fragment of the heterodimer. The membrane-anchored receptor fragment is cleaved at S3 by the γ secretase complex, an intramembrane aspartyl protease that cleaves its substrates within their transmembrane domains, to release the Notch intracellular domain (NICD) [9]. The released NICD is then translocated to the nucleus, where it interacts and forms a complex with the CSL family [CBF1, Su(H), and Lag-1] of transcriptional regulators, the transactivator mastermind-like (MAML), and other modulators [9]. After its formation, the complex activates the transcription of multiple effector genes, including members of the *HES*/*HEY* family [10]. In contrast, noncanonical functions of Notch that are independent of ligand binding or transcription have also been reported [11]. Previous studies have reported that the noncanonical Notch pathway may function through interactions with other signaling pathways, including WNT, NF-kappa B, and JNK [12, 13]. However, information about the noncanonical Notch signaling pathway remains poorly understood due to a lack of mechanistic understanding [14].

The involvement of the Notch signaling pathway in ovarian follicle development and oocyte maturation has been proposed. Previous studies in mouse ovaries demonstrated that the Notch receptors (NOTCH1–3) and Notch ligand JAG2 are expressed in granulosa cells, while JAG1 and JAG2 are expressed in the oocytes [10, 15]. Recently, it has been reported that transcripts of *NOTCH1*, *JAG2*, *HES1*, and *HES2* are expressed in bovine germinal vesicle oocytes [12]. Furthermore, Manosalva et al. [16] demonstrated that *Hes1*, a target gene of the Notch signaling pathway, regulates the development of ovarian somatic cells that are essential for oocyte maturation and survival. In that study, conventional and conditional *Hes1* knockout in ovarian somatic cells and chemical inhibition of the Notch signaling pathway in ovaries using a γ secretase inhibitor led to decreases in the total number, size, and maturation of oocytes in mice.

Although the previous study implied that the Notch signaling pathway may be required for mammalian oocyte maturation, the exact role of the pathway in this process has not been fully elucidated. Therefore, the aims of this study were to determine the existence and role of the Notch signaling pathway during porcine oocyte maturation. To this end, we investigated the existence of transcripts and proteins of Notch ligands (JAG1 and 2 and DLL1, 3, and 4) and receptors (NOTCH1–4) in porcine cumulus–oocyte complexes (COCs). Additionally, RO4929097 (RO), an inhibitor of γ secretase, was used to determine the effects of Notch signaling inhibition on porcine oocyte maturation.

Materials and methods

Chemicals

Unless otherwise stated, all chemicals and reagents used were purchased from Sigma-Aldrich (St. Louis, MO, USA).

Oocyte recovery and in vitro maturation

Porcine ovaries were obtained from a local slaughterhouse, placed in 0.9% physiological saline at 38.5 °C, and transported to the laboratory within 2 h. Using a syringe, COCs were collected from the surface of the ovarian follicles (3–7 mm in diameter), and those containing three or more intact cumulus layers were selected. The COCs were rinsed three times with an in vitro maturation (IVM) medium composed of tissue culture medium 199, 10 ng/mL epidermal growth factor, 25 μM β-mercaptoethanol, 0.57 mM cysteine, 10% porcine follicular fluid, 10 IU/mL

pregnant mare serum gonadotropin (PMSG; ProSpec, Rehovot, Israel), and 10 IU/mL human chorionic gonadotropin (hCG; ProSpec). Approximately 50 COCs were incubated in IVM medium with paraffin oil (Junsei, Tokyo, Japan) for 22 h at 38.5 °C under 5% CO_2. Thereafter, the COCs were transferred to PMSG- and hCG-free IVM medium and incubated for another 22 h at 38.5 °C under 5% CO_2.

Chemical treatment

A stock solution of 20 mM RO (Selleckchem, Houston, TX, USA) was prepared with dimethylsulfoxide and diluted in IVM medium to final concentrations of 0, 5, 10, and 20 μM.

Assessment of the cumulus expansion and nuclear maturation of oocytes

A total of 1000 COCs was used in five independent replicates. After 44 h of IVM, cumulus expansion was evaluated on the basis of the morphology of the COCs and classified into four levels: degree 1 (cumulus cells that are spherical and compacted with minimal observable expansion), degree 2 (cumulus cells that are partially expanded with an outer layer), degree 3 (cumulus cells that are mostly expanded except for the corona radiata), and degree 4 (cumulus cells that are fully expanded). To determine the nuclear maturation of the oocytes after 44 h of IVM, the COCs were placed in a denuding medium containing Dulbecco's phosphate-buffered saline (DPBS; Gibco, Grand Island, NY, USA), 100 μg/mL penicillin G, 75 μg/mL streptomycin sulfate, and 0.1% hyaluronidase. After gently pipetting the COCs, the denuded oocytes were observed under a microscope (Nikon Corp., Tokyo, Japan) and classified as immature (without polar body extrusion), metaphase II (MII; with polar body extrusion), or degenerate.

Parthenogenetic activation and in vitro culture

A total of 631 MII oocytes was used in five independent replicates. For parthenogenetic activation, MII oocytes were treated with 15 μM of ionomycin in DPBS (Gibco) supplemented with 60 μg/mL gentamicin sulfate, 75 μg/mL streptomycin sulfate, and 4 mg/mL bovine serum albumin (BSA) for 5 min in the dark. After activation, the oocytes were incubated in in vitro culture medium (PZM-3 medium containing 4 mg/mL BSA) supplemented with 5 μg/mL cytochalasin B and 2 mM 6-dimethylaminopurine for 4 h at 38.5 °C under 5% CO_2. Subsequently, the oocytes were transferred to fresh in vitro culture medium and cultured for 6 days at 38.5 °C under 5% CO_2.

Immunocytochemistry

For NOTCH1 staining, in total, 49, 50, 48, and 48 COCs were sampled at different time points (0, 22, 28, and 44 h of IVM, respectively) and used in four independent replicates. For NOTCH2 staining, in total, 43, 48, 46, and 47 COCs were sampled at different time points (0, 22, 28, and 44 h of IVM, respectively) and used in four independent replicates. For NOTCH3 staining, in total, 35, 36, 37, and 35 COCs were sampled at different time points (0, 22, 28, and 44 h of IVM, respectively) and used in four independent replicates. For NOTCH4 staining, in total, 45, 43, 45, and 43 COCs were sampled at different time points (0, 22, 28, and 44 h of IVM, respectively) and used in four independent replicates. For JAG1 staining, in total, 43, 43, 40, and 44 COCs were sampled at different time points (0, 22, 28, and 44 h of IVM, respectively) and used in four independent replicates. For JAG2 staining, in total, 49, 46, 47, and 48 COCs were sampled at different time points (0, 22, 28, and 44 h of IVM, respectively) and used in four independent replicates. For DLL1 staining, in total, 39, 38, 38, and 38 COCs were sampled at different time points (0, 22, 28, and 44 h of IVM, respectively) and used in three independent replicates. For DLL3 staining, in total, 42, 41, 38, and 38 COCs were sampled at different time points (0, 22, 28, and 44 h of IVM, respectively) and used in three independent replicates. For DLL4 staining, in total, 42, 41, 42, and 39 COCs were sampled at different time points (0, 22, 28, and 44 h of IVM, respectively) and used in three independent replicates. For GDF9 staining, a total of 40 MII oocytes was used in three independent replicates. For BMP15 staining, a total of 40 MII oocytes was used in three independent replicates. For CDX2 staining, a total of 66 blastocysts was used in three independent replicates. For α-Tubulin staining to evaluate the proportions of Pro-MI and MI stage oocytes, a total of 348 oocytes was used in five independent replicates. For α-Tubulin staining to evaluate the chromosome and spindle morphology, a total of 144 oocytes was used in four independent replicates. For BUBR1 staining, a total of 96 oocytes was used in three independent replicates. For Ac-Tubulin staining, a total of 70 oocytes was used in three independent replicates. For HES1 staining, a total of 60 COCs was used in three independent replicates. For HES2 staining, a total of 42 COCs was used in three independent replicates. For HEY1 staining, a total of 54 COCs was used in three independent replicates. For HEY2 staining, a total of 60 COCs was used in three independent replicates. COCs, oocytes, and blastocysts were washed three times in DPBS (Welgene, Daegu, Republic of Korea) supplemented with 0.1% polyvinyl alcohol (PBS-PVA) and then fixed overnight in 4% paraformaldehyde at 4 °C. After washing three times with PBS-PVA, the respective cells

were incubated in PBS supplemented with 1% Triton X-100 for 1 h at ambient temperature. Then, the permeabilized samples were washed three times with PBS-PVA. Subsequently, the cell samples were placed in PBS-PVA containing 1 mg/mL BSA (PBS-PVA-BSA) at ambient temperature for 1 h to block nonspecific binding. To stain for caudal type homeobox 2 (CDX2), blastocysts were further incubated in PBS containing 10% normal goat serum for 1 h. The cell samples were incubated with primary antibodies overnight at 4 °C. The specific antibodies used are listed in Supplementary Table 1. After washing three times with PBS-PVA-BSA, the samples were treated with Alexa Fluor 488-labeled goat anti-rabbit, goat anti-mouse, or donkey anti-goat IgG secondary antibodies (Invitrogen, Waltham, MA, USA) for 1 h at ambient temperature. Following this, the samples were washed three times with PBS-PVA-BSA and mounted on glass slides with mounting solution containing 1.5 μg/mL 4′,6-diamidino-2-phenylindole (DAPI; Vector Laboratories, Newark, CA, USA). Cell fluorescence was observed using a laser scanning confocal fluorescence microscope (LSM700; Carl Zeiss, Oberkochen, Germany) or a fluorescence microscope (DMi8; Leica Microsystems, Wetzlar, Germany), and the fluorescence intensity was analyzed using ImageJ software after normalization through subtraction of the background intensity to that of control.

Terminal deoxynucleotidyl transferase-mediated dUTP-digoxygenin nick end-labeling assay

A total of 80 blastocysts was used in five independent replicates. The In Situ Cell Death Detection Kit (Roche, Basel, Switzerland) was used for the terminal deoxynucleotidyl transferase-mediated dUTP-digoxygenin nick end-labeling (TUNEL) assay. Blastocysts were fixed overnight in 4% paraformaldehyde at 4 °C, then washed three times with PBS-PVA, and subsequently permeabilized in DPBS with 1% (v/v) Triton X-100 for 1 h at ambient temperature. Thereafter, the blastocysts were washed three times with PBS-PVA and incubated with fluorescein-conjugated dUTP and terminal deoxynucleotidyl transferase for 1 h at 38.5 °C. After the incubation, the blastocysts were washed three times with PBS-PVA and then mounted on slides with mounting solution containing 1.5 μg/mL DAPI (Vector Laboratories). Cell fluorescence was observed using a fluorescence microscope (DMi8; Leica Microsystems).

Reverse transcription and quantitative polymerase chain reactions

Poly(A) mRNAs were isolated from cumulus cells, oocytes, and blastocysts using the Dynabeads mRNA Direct Kit (Invitrogen) following the manufacturer's protocol and then reverse transcribed using the PrimeScript™ RT Reagent Kit with gDNA Eraser (Takara Bio Inc., Shiga, Japan) according to the manufacturer's protocol. A total of 50 COCs or 10 blastocysts were sampled in each batch for Poly(A) mRNA extraction and used in three independent replicates. For the reverse transcription polymerase chain reactions (RT-PCR), a SureCycler 8800 system (Agilent Technologies, Santa Clara, CA, USA) was used: 3 μl cDNA, 1 μl (5 pM) forward primer, 1 μl (5 pM) reverse primer, 10 μl ExPrime Premix (GeNet Bio, Daejeon, Republic of Korea), and 5 μl of Nuclease-free water (Invitrogen). The PCR products were electrophoresed for 30 min at 110 V using a JY600 Basic Power Supply (JUNYI, Beijing, China). The results were visualized and photographed using a gel imaging system (Fusion SOLO S; Vilber, Marne La Vallée, France). SYBR Premix Ex Taq (TaKaRa Bio) and the AriaMx Real-time PCR system (Agilent) were used for the quantitative PCR: 3 μl cDNA, 1 μl (5 pM) forward primer, 1 μl (5 pM) reverse primer, and 5 μl SYBR Premix Ex Taq (TaKaRa Bio). Glyceraldehyde-3-phosphate dehydrogenase (*GAPDH*) was used as the internal standard for comparative analyses. The specific primers used for the PCRs are listed in Supplementary Table 2.

Chromosome spreading

A total of 226 oocytes was used in six independent replicates. To spread the chromosomes, the oocytes were treated with acidic Tyrode's solution to remove the zona pellucida. After a brief recovery in fresh medium, the oocytes were fixed and spread on glass slides using 1% paraformaldehyde in distilled water (pH 9.2) containing 0.15% Triton X-100 and 3 mM dithiothreitol. The slide samples were dried slowly for several hours at ambient temperature in a humid chamber, following which they were covered with a blocking solution for 1 h at ambient temperature. Then, the cells were incubated first with BUBR1 antibody (Abcam, Cambridge, UK) overnight at 4 °C and then with Alexa Fluor 488-labeled goat anti-rabbit secondary antibody for 1 h at ambient temperature. Finally, the DNA was stained by dropping 10 μL of mounting solution containing 1.5 μg/mL DAPI (Vector Laboratories) onto the cells. Cell fluorescence was examined using a laser scanning confocal fluorescence microscope (LSM700; Carl Zeiss).

Analysis of actin filaments

A total of 279 MII oocytes was used in three independent replicates. MII oocytes were fixed overnight with 4% paraformaldehyde at 4 °C, then incubated in DPBS containing 1% Triton X-100 for 1 h at ambient temperature, and subsequently blocked with 2 mg/mL BSA in PBS-PVA for 1 h at ambient temperature. Then, the oocytes were

treated with 10 μg/mL phalloidin-tetramethylrhodamine B isothiocyanate for 2 h at ambient temperature. After washing in PBS-PVA, the oocytes were mounted onto glass slides with a mounting solution containing 1.5 μg/mL DAPI and observed using a laser scanning confocal fluorescence microscope (LSM700; Zeiss).

Analysis of mitochondria and endoplasmic reticula

For MitoTracker staining, a total of 156 MII oocytes was used in five independent replicates. For JC-1 staining, a total of 96 MII oocytes was used in three independent replicates. For ER-Tracker staining, a total of 236 MII oocytes was used in nine independent replicates. To assess the mitochondrial and endoplasmic reticulum (ER) activities, MII oocytes were incubated in IVM medium containing 200 nM MitoTracker Red CMXRos (Invitrogen), JC-1 (1:100) (Cayman Chemical, Ann Arbor, MI, USA), or 1 μM ER-Tracker (Invitrogen) for 1 h. Subsequently, the oocytes were washed three times with PBS-PVA (10 min each time) and then fixed in 4% paraformaldehyde for 2 h at 38.5 °C. Cell fluorescence was observed immediately using a fluorescence microscope (DMi8; Leica Microsystems). To determine mitochondrial and ER distribution, stained and fixed oocytes were washed three times in PBS-PVA and then mounted onto glass slides using mounting solution containing 1.5 μg/mL DAPI (Vector Laboratories). Cell fluorescence was observed immediately under a fluorescence microscope (DMi8; Leica Microsystems), and the fluorescence intensity was analyzed using ImageJ software after normalization through subtraction of the background intensity to that of control.

Analysis of ATP and cytoplasmic and mitochondrial calcium concentrations

For ATP staining, a total of 80 MII oocytes was used in three independent replicates. For Fluo-3 staining, a total of 100 MII oocytes was used in four independent replicates. For Rhod-2 staining, a total of 160 MII oocytes was used in five independent replicates. MII oocytes were washed three times with PBS-PVA and then fixed overnight in 4% paraformaldehyde at 4 °C. To stain ATP, fixed oocytes were washed three times with PBS-PVA and then incubated in PBS-PVA containing 500 nM BODIPY FL ATP (Molecular Probes, Eugene, OR, USA) for 1 h in the dark at ambient temperature. Subsequently, the oocytes were washed three times with PBS-PVA and then mounted onto glass slides with a mounting solution containing 1.5 μg/mL DAPI. To stain cytoplasmic and mitochondrial calcium, the fixed oocytes were washed three times with PBS-PVA and then incubated in PBS-PVA containing 10 μM Fluo-3 (Invitrogen) and 5 μM Rhod-2 (Invitrogen) for 1 h in the dark at ambient temperature. Sample fluorescence was observed using a fluorescence microscope (DMi8; Leica Microsystems), and the fluorescence intensity was analyzed using ImageJ software after normalization through subtraction of the background intensity to that of control.

Statistical analysis

All statistical analyses were performed using SigmaStat software (SPSS Inc., Chicago, IL, USA). Each experiment was conducted at least three times. One-way analysis of variance was used for comparisons among three or more groups, followed by Tukey's post-hoc test. Student's t-test was used to compare the scores between two groups. The results are presented as the mean ± standard error of the mean. Differences were considered statistically significant at a *P*-value of less than 0.05.

Results

Notch signaling-related receptors and ligands are expressed during meiotic progression in porcine oocytes and cumulus cells

To determine the existence of the Notch signaling pathway in oocyte meiotic maturation, we first analyzed the subcellular localization and expression of the pathway-related proteins at 0, 22, 28, and 44 h of IVM. Immunofluorescence analyses continuously detected Notch signaling-related receptors (NOTCH1–4) and ligands (JAG1 and 2 and DLL1, 3, and 4) in the oocytes and cumulus cells throughout IVM (Fig. 1A–D). RT-PCR analyses also confirmed the presence of transcripts of these Notch receptors and ligands in oocytes and cumulus cells throughout IVM (Fig. 1E). These results suggest that Notch signaling may have notable effects on oocyte meiotic progression.

Notch signaling is essential for oocyte meiotic progression

To investigate the effects of Notch signaling inhibition on oocyte meiotic maturation, we cultured COCs in maturation media containing different concentrations of RO (0, 5, 10, and 20 μM) and then evaluated the cumulus cell expansion and oocyte nuclear maturation. RO treatment significantly decreased the proportion of degree 4 cumulus expansion and increased that of degree 3 in a dose-dependent manner, which was notable starting from 10 μM inhibitor treatment (Fig. 2A, B). Additionally, the transcript levels of cumulus expansion-related genes [hyaluronan synthase 2 (*SHAS2*), prostaglandin G/H synthase 1 (*PTGS1*), *PTGS2*, and tumor necrosis factor-inducible gene 6 protein (*TNFAIP6*)] were significantly lower in the 10 μM RO-treated cumulus cells than in the controls (Fig. 2C). RO treatment significantly decreased the proportion of MII oocytes and increased that of immature oocytes in a dose-dependent manner

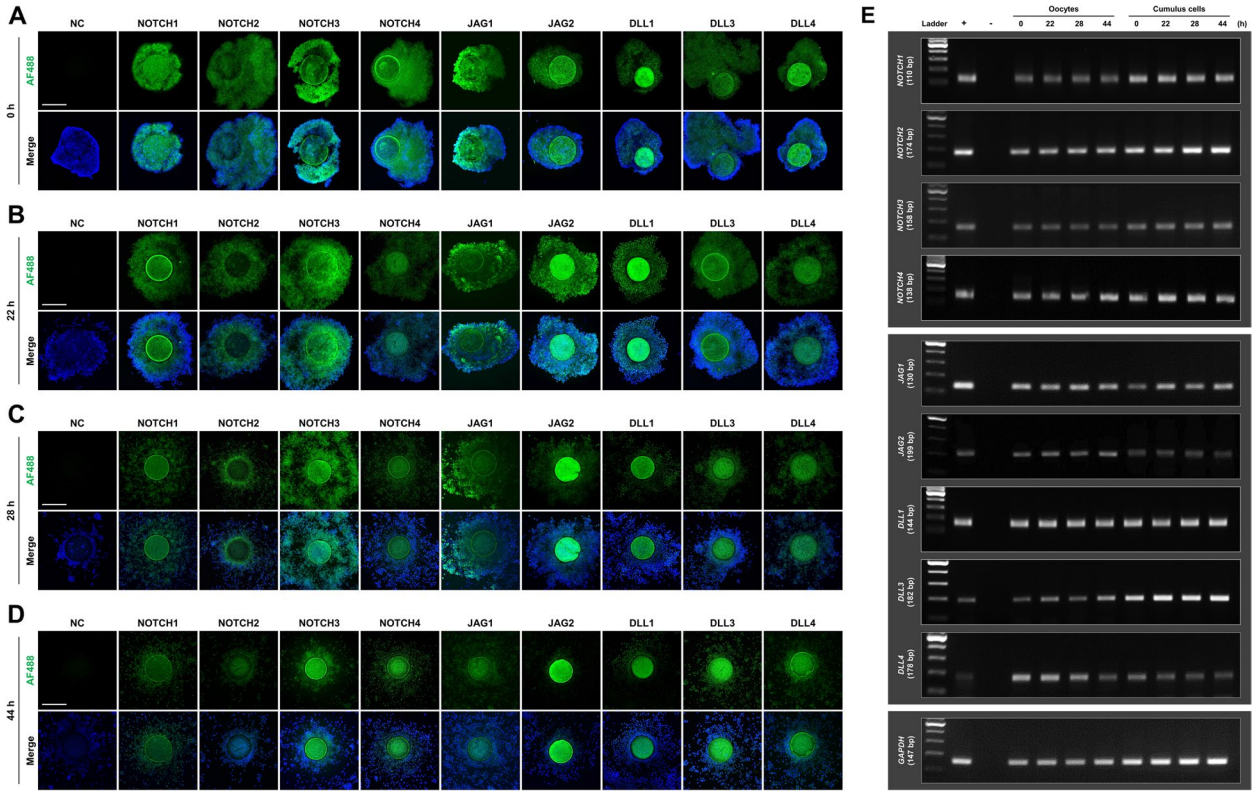

Fig. 1 Subcellular localization and expression of the Notch signaling pathway during porcine oocyte meiotic progression. Immunofluorescence analyses of Notch signaling receptors (NOTCH1, NOTCH2, NOTCH3, and NOTCH4) and ligands (JAG1, JAG2, DLL1, DLL3, and DLL4) in porcine cumulus–oocyte complexes (COCs) at (**A**) 0, (**B**) 22, (**C**) 28, and (**D**) 44 h of in vitro maturation (IVM). Bar = 200 μm. **E** RT-PCR analyses of Notch signaling receptors (*NOTCH1*, *NOTCH2*, *NOTCH3*, and *NOTCH4*) and ligands (*JAG1*, *JAG2*, *DLL1*, *DLL3*, and *DLL4*) in oocytes and cumulus cells at 0, 22, 28, and 44 h of IVM. Each RT-PCR experiment was performed using oocytes and cumulus cells isolated from 50 COCs

(Fig. 2D, E and Supplementary Table 3). In particular, the transcript levels of genes related to oocyte competence [growth/differentiation factor 9 (*GDF9*) and bone morphogenetic protein 15 (*BMP15*)], mitogen-activated protein kinase (*MOS*), and maturation promoting factor [G2/mitotic-specific cyclin B1 (*CCNB1*) and cyclin-dependent kinase 1 (*CDK1*)] were significantly lower in the 10 μM RO-treated group than in the control group (Fig. 2F). Consistent with the qRT-PCR results, the levels of GDF9 and BMP15 proteins were significantly decreased in the 10 μM RO-treated group relative to the control group (Fig. 2G–J). These results suggest that Notch signaling plays an important regulatory role in porcine oocyte meiotic progression.

Inhibition of Notch signaling during in vitro maturation reduces the developmental competence of parthenogenetically activated embryos

To investigate the effect of Notch signaling inhibition during IVM on early porcine embryogenesis, RO-treated MII oocytes were parthenogenetically activated, and the developmental competence of the parthenotes was evaluated. The rates of cleavage and blastocyst formation were significantly decreased in a dose-dependent manner in the RO-treated MII oocytes (Fig. 3A–C and Supplementary Table 4). The developmental kinetics during the preimplantation period were delayed in the RO-treated MII oocytes compared with that in the control. In particular, the proportion of expanded blastocysts was significantly lower than that of the controls, leading to a decrease in the total cell number (Fig. 3D–G and Supplementary Tables 4 and 5). Additionally, we evaluated the quality of the blastocysts using CDX2 staining and TUNEL assays. The apoptotic rate was significantly higher in the 10 μM RO-treated group than in the control group (Fig. 3H, I and Supplementary Table 6). Although there was no significant difference in the transcript levels of the pro-apoptotic gene [BCL2-associated X (*BAX*)] between the two groups, the transcript level of the anti-apoptotic gene [BCL2-like protein 1 (*BCL2L1*)] was significantly lower in the 10 μM RO-treated group (Fig. 3J). Moreover, the cell numbers of the inner cell mass and trophectoderm were significantly lower in the 10 μM RO-treated group (Fig. 3K, L and Supplementary Table 7), as were the transcript levels of developmental

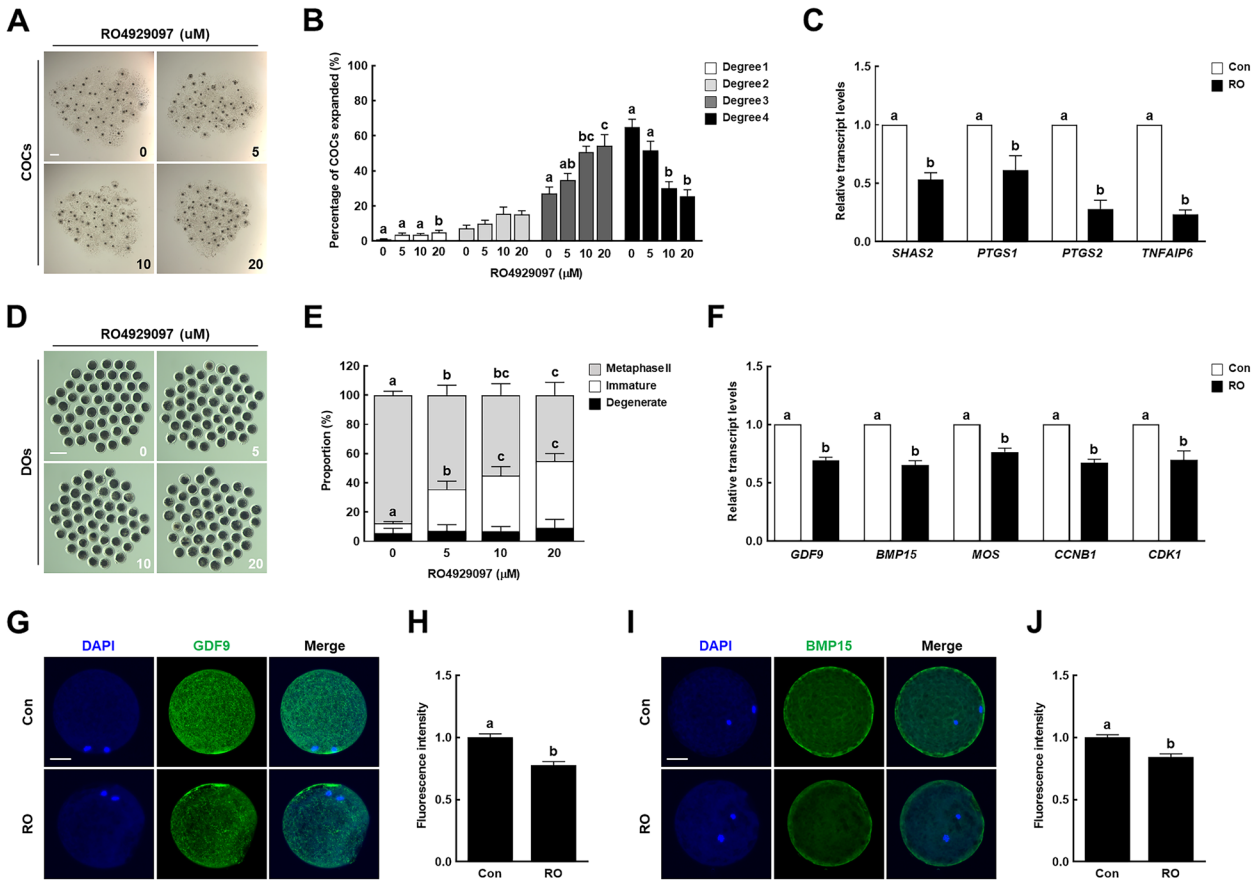

Fig. 2 Effect of Notch signaling inhibition on porcine oocyte meiotic progression. **A** Representative images and (**B**) proportions of cumulus cell expansion in the control and RO4929097-treated groups after 44 h of in vitro maturation (IVM) ($n = 250$ per group). Bar = 200 μm. **C** qRT-PCR-assayed transcript levels of cumulus expansion-related genes (*SHAS2*, *PTGS1*, *PTGS2*, and *TNFAIP6*) in cumulus cells after 44 h of IVM in the indicated groups ($n = 3$ per group). **D** Representative images and (**E**) proportions of different stages of denuded oocytes in the control and RO4929097-treated groups after 44 h of IVM ($n = 250$ per group). Bar = 200 μm. **F** qRT-PCR-assayed transcript levels of genes related to oocyte competence (*GDF9* and *BMP15*), mitogen-activated protein kinase (*MOS*), and maturation promoting factor (*CCNB1* and *CDK1*) in oocytes after 44 h of IVM in the indicated groups ($n = 3$ per group). **G** Representative images and (**H**) fluorescence intensity of GDF9 immunocytochemical staining in oocytes in the indicated groups ($n = 20$ per group). Bar = 50 μm. **I** Representative images and (**J**) fluorescence intensity of BMP15 immunocytochemical staining in oocytes in the indicated groups ($n = 20$ per group). Bar = 50 μm. Data are derived from at least three independent experiments, and different superscripts indicate significant differences ($P < 0.05$). Con, control; RO, 10 μM RO4929097

potential-related genes [POU domain, class 5, transcription factor 1 (*POU5F1*), *NANOG*, SRY-box transcription factor 2 (*SOX2*), *CDX2*, transcriptional enhancer factor TEF-3 (*TEAD4*), and GATA-binding protein 3 (*GATA3*)] (Fig. 3M). On the basis of these results, 10 μM was selected as the RO concentration for subsequent experiments. Taken together, these results suggest that the inhibition of Notch signaling during IVM reduces the quality of porcine oocytes, leading to the failure of early embryogenesis.

Notch signaling is important for cell cycle progression, spindle assembly, and chromosome alignment during oocyte meiotic progression

To determine how Notch signaling affects the nuclear maturation of porcine oocytes, we examined their cell cycle entry following RO treatment. After 44 h of IVM, most of the control oocytes had matured to the MII stage, whereas the RO-treated oocytes were arrested at the germinal vesicle breakdown or metaphase I (MI) stages

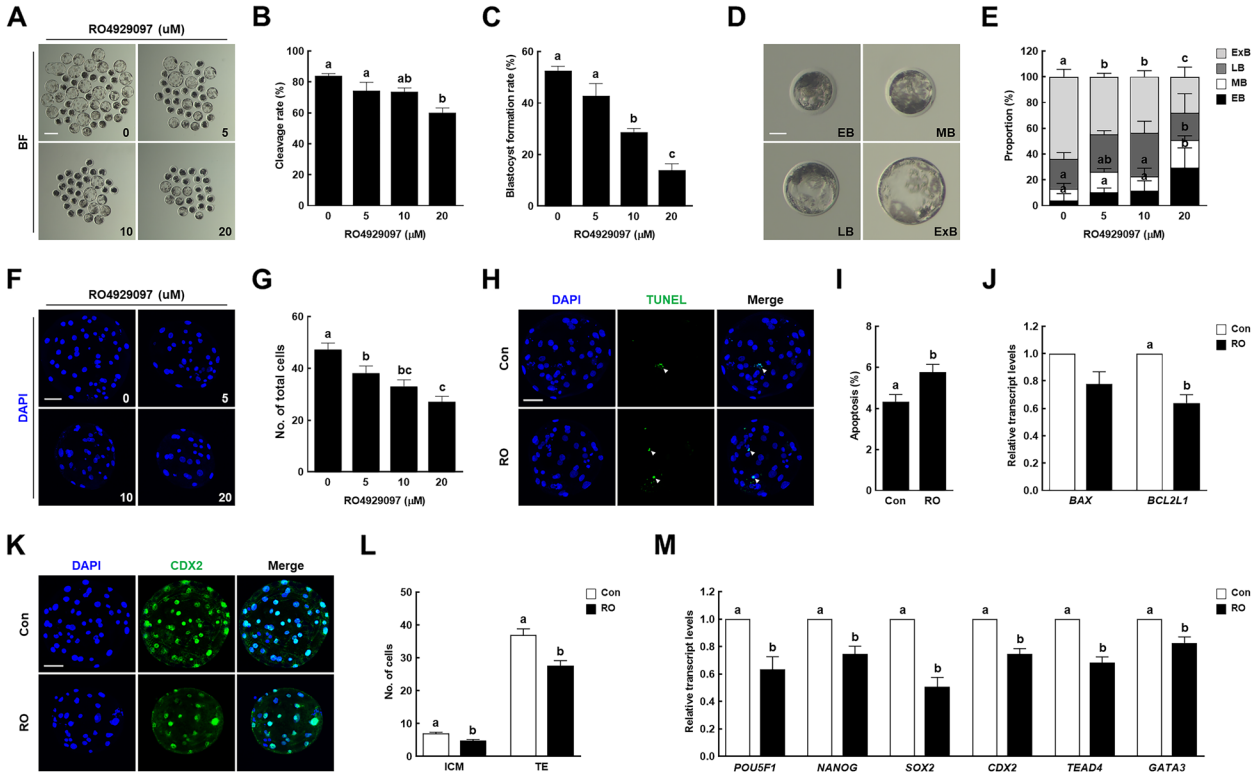

Fig. 3 Effect of Notch signaling inhibition during IVM on early porcine embryogenesis. **A** Representative images of blastocysts developed from control and RO4929097-treated groups after parthenogenetic activation. Bar = 200 μm. **B** Cleavage and (**C**) blastocyst formation rates of embryos from control and RO4929097-treated groups after parthenogenetic activation (0: $n = 219$; 5: $n = 161$; 10: $n = 138$; 20: $n = 113$). **D** Representative images of blastocysts at four different stages: early blastocyst (EB), middle blastocyst (MB), large blastocyst (LB), and expanded blastocyst (ExB). Bar = 50 μm. **E** Proportions of various blastocyst stages in the control and RO4929097-treated groups (0: $n = 133$; 5: $n = 87$; 10: $n = 51$; 20: $n = 40$). **F** Representative nuclear-stained images of blastocysts in the control and RO4929097-treated groups. Bar = 50 μm. **G** Quantification of total cell numbers in the control and RO4929097-treated groups ($n = 20$ per group). **H** Representative images of TdT-mediated dUTP nick-end labeling (TUNEL)-stained blastocysts. Bar = 50 μm. Embryos were subjected to TUNEL (green, white arrow) and nuclear staining (blue). **I** Quantification of the proportion of apoptotic cells in the indicated groups ($n = 40$ per group). **J** qRT-PCR-assayed transcript levels of apoptosis-related genes (*BAX* and *BCL2L1*) in blastocysts in the indicated groups ($n = 3$ per group). **K** Representative images of CDX2 staining in blastocysts. Bar = 50 μm. **L** Quantification of cell numbers in the inner cell mass and trophectoderm in the indicated groups ($n = 33$ per group). **M** qRT-PCR-assayed transcript levels of developmental potential-related genes (*POU5F1*, *NANOG*, *SOX2*, *CDX2*, *TEAD4*, and *GATA3*) in blastocysts in the indicated groups ($n = 3$ per group). Data are derived from at least three independent experiments, and different superscripts indicate significant differences ($P < 0.05$). Con, control; RO, 10 μM RO4929097

(Fig. 4A, B). Although some of the RO-treated oocytes matured to the MII stage, they showed a substantially higher incidence of aneuploidy and higher proportion of abnormal actin morphology compared with the controls (Fig. 4C–F). Moreover, we found that the majority of RO-treated oocytes were arrested at the Pro-MI stage at 28 h of IVM (Fig. 4G, H) and, interestingly, showed noticeably reduced levels of BUBR1, which plays a role in the mitotic spindle assembly checkpoint and protects against aneuploidy by ensuring proper chromosomal segregation (Fig. 4I, J). On the basis of these results, we analyzed the meiotic spindle and chromosome organization in MI stage oocytes following RO treatment. The control oocytes had typical barrel-shaped spindles containing well-aligned chromosomes. By contrast, a significantly high proportion of RO-treated oocytes had aberrant spindles or misaligned chromosomes (Fig. 4K–M). Moreover, the RO treatment significantly increased the number of lagging chromosomes (Fig. 4N). Our further analysis of the spindle width, spindle length, metaphase plate width, and the ratio of metaphase plate width to spindle length revealed that these parameters were all notably increased in the RO-treated oocytes relative to their values in the controls (Fig. 4O–S). We also confirmed that RO treatment significantly reduced the acetylated tubulin level (Fig. 4T, U). Taken together, these results indicate that Notch signaling plays a crucial role

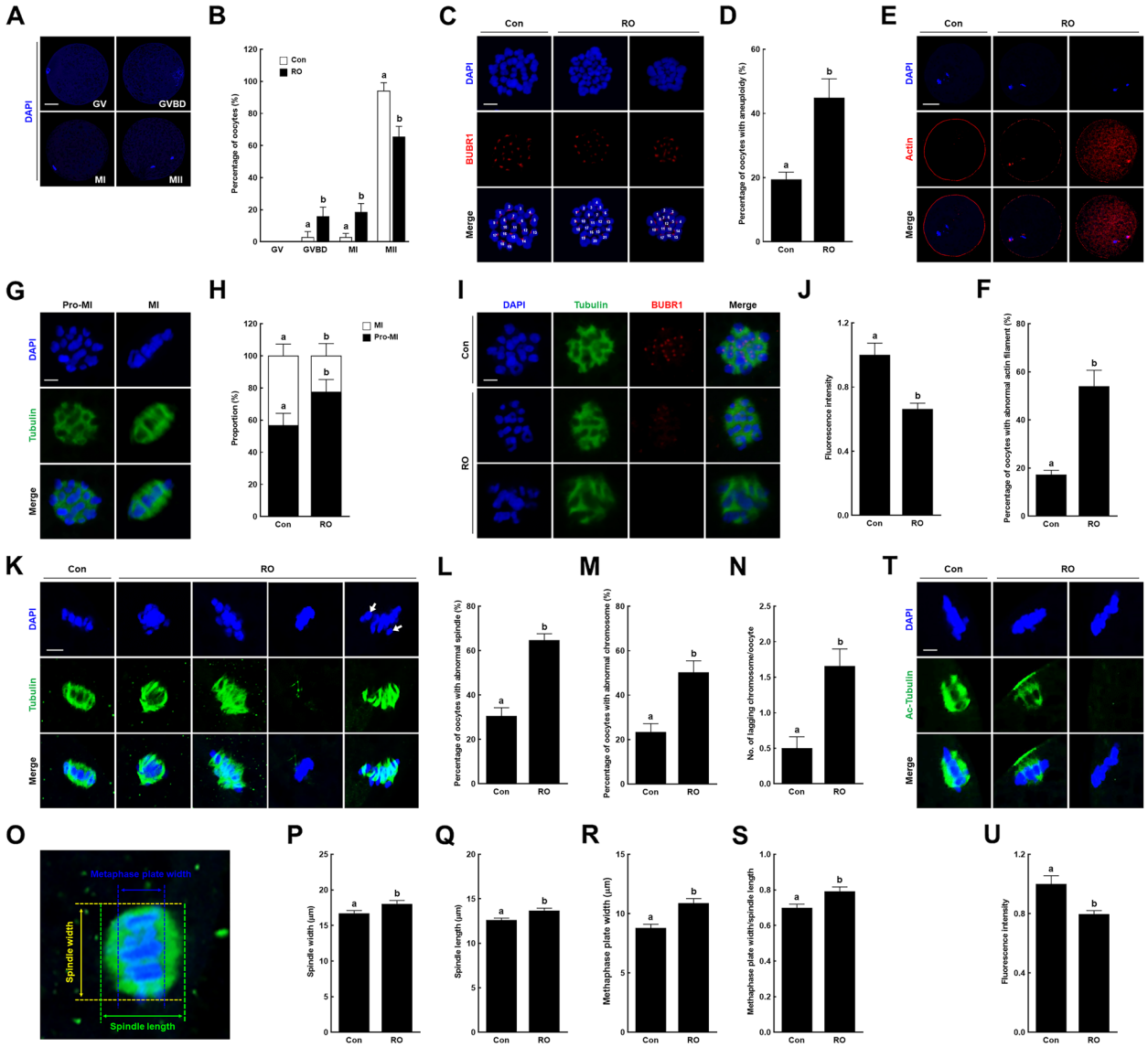

Fig. 4 Effects of Notch signaling inhibition on cell cycle progression, spindle assembly, and chromosome alignment in porcine oocytes. **A** Representative images of oocytes at four various stages: germinal vesicle (GV), germinal vesicle breakdown (GVBD), metaphase I (MI), and metaphase II (MII). Bar = 50 μm. **B** Proportions of oocyte stages at 44 h of in vitro maturation (IVM) in the indicated groups (con: $n = 238$; RO: $n = 226$). **C** Representative images of chromosome spreading in MII oocytes in the indicated groups. Bar = 5 μm. **D** Proportions of MII oocytes with aneuploidy in the indicated groups (con: $n = 135$; RO: $n = 91$). **E** Representative images of MII oocytes stained for actin filaments in the indicated groups. Bar = 50 μm. **F** Proportions of MII oocytes with abnormal actin filaments in the indicated groups (con: $n = 145$; RO: $n = 134$). **G** Representative images of Pro-MI and MI stage oocytes. Bar = 5 μm. **H** Proportions of Pro-MI and MI stage oocytes at 28 h of IVM in the indicated groups (con: $n = 175$; RO: $n = 173$). **I** Representative images and (**J**) fluorescence intensity of BUBR1 staining in Pro-MI stage oocytes in the indicated groups ($n = 48$ per group). Bar = 5 μm. **K** Representative images of the spindle and chromosome structures in the indicated groups. Bar = 5 μm. White arrows indicate lagging chromosomes. Proportions of oocytes with abnormal (**L**) spindle and (**M**) chromosome morphology in the indicated groups (con: $n = 65$; RO: $n = 79$). **N** Quantification of lagging chromosomes per oocyte in the indicated groups ($n = 50$ per group). **O** Representative images of spindles and chromosomes indicating the spindle width and length and metaphase plate width. Bar = 5 μm. Quantification of the (**P**) spindle width, (**Q**) spindle length, (**R**) metaphase plate width, and (**S**) ratio of the metaphase plate width to spindle length in the indicated groups ($n = 50$ per group). **T** Representative images and (**U**) fluorescence intensity of acetylated tubulin staining in oocytes in the indicated groups ($n = 35$ per group). Bar = 5 μm. Data are derived from at least three independent experiments, and different superscripts indicate significant differences ($P < 0.05$). Con, control; RO, 10 μM RO4929097

in microtubule function, including spindle organization and chromosome segregation, during oocyte meiotic progression.

Notch signaling maintains organelle distribution and functions in porcine oocytes

During oocyte maturation, the movement and distribution of mitochondria and endoplasmic reticula (ERs) depend on microtubule dynamics, and the functions of these organelles are important features of oocyte cytoplasmic maturation. Thus, we assessed the effect of Notch signaling inhibition on mitochondrial and ER distribution and functions in porcine oocytes. In RO-treated oocytes, the mitochondrial content was lower and the proportion of abnormal mitochondrial distribution was higher than those in the controls (Fig. 5A–D). Mitochondrial function analysis revealed that the RO-treated oocytes showed significantly lower mitochondrial membrane potentials, ATP contents, and transcript levels of mitochondrial biogenesis- and function-related genes [transcription factor A, mitochondrial (*TFAM*), DNA polymerase gamma (*POLG*), *POLG2*, sirtuin 1 (*SIRT1*), peroxisome proliferator-activated receptor gamma coactivator 1-alpha (*PPARGC1A*), carnitine palmitoyltransferase 1 (*CPT1A*), and carnitine *O*-palmitoyltransferase 1, muscle isoform (*CPT1B*)] than those of the controls (Fig. 5E–I). Similarly, the RO-treated oocytes had a lower ER content and higher proportion of abnormal ER distribution than those of the controls (Fig. 5J–M). Moreover, the intracellular and mitochondrial calcium ion levels were significantly higher in the RO-treated oocytes (Fig. 5N–Q). Additionally, the transcript levels of ER stress-related genes [endoplasmic reticulum chaperone BiP (*HSPA5*), non-specific serine/threonine protein kinase (*ERN1*), activating transcription factor 6 (*ATF6*), DNA damage-inducible transcript 3 protein (*DDIT3*), and cyclic AMP-dependent transcription factor ATF-4 (*ATF4*)] and the spliced/unspliced X-box binding protein 1 (*XBP1*) gene ratio were significantly higher in the RO-treated oocytes (Fig. 5R, S). These results suggest that Notch signaling supports proper cytoplasmic maturation by regulating the mitochondrial and ER systems during oocyte meiotic progression.

Canonical Notch signaling is active during oocyte meiotic progression

The HES and HEY families of transcription factors act primarily downstream of the canonical Notch signaling pathway. To verify that Notch regulation of porcine meiotic progression occurs downstream of the signaling pathway, we investigated the transcript and protein levels of the HES1/2 and HEY1/2 families following RO treatment. Immunofluorescence and qRT-PCR analyses showed that all Notch signaling pathways downstream targets, HES1/2 and HEY1/2, were markedly downregulated in oocytes and cumulus cells following RO treatment (Fig. 6), indicating that the canonical Notch signaling pathway is active through downstream targets during oocyte meiotic progression.

Discussion

In this study, we investigated the functional roles and potential regulatory mechanisms of the Notch signaling pathway during porcine oocyte meiotic maturation. Notch signaling-related transcripts and proteins were continuously detected in oocytes and cumulus cells during meiotic maturation. To inhibit Notch activity, we treated COCs with an inhibitor of γ secretase and observed the negative effects on cumulus cell expansion, oocyte nuclear maturation, and subsequent embryo development. These meiotic defects provided proof that Notch signaling promotes oocyte nuclear maturation by orchestrating cell cycle progression, spindle organization, and chromosome segregation. Moreover, we found that Notch signaling ensures proper cytoplasmic maturation of oocytes by regulating the mitochondrial and ER

(See figure on next page.)

Fig. 5 Effects of Notch signaling inhibition on the distribution and functions of the mitochondria and endoplasmic reticula in porcine oocytes. **A** Representative images and (**B**) fluorescence intensity of MitoTracker-stained oocytes in the indicated groups ($n = 78$ per group). Bar = 100 μm. **C** Representative images of mitochondrial distribution in oocytes and (**D**) the proportions of oocytes with abnormal mitochondrial distribution in the indicated groups ($n = 3$ per group). Bar = 50 μm. **E** Representative images and (**F**) fluorescence intensity (red/green) of JC-1-stained oocytes in the indicated groups ($n = 48$ per group). Bar = 100 μm. **G** Representative images and (**H**) fluorescence intensity of BODYPY-ATP-stained oocytes in the indicated groups ($n = 40$ per group). Bar = 50 μm. **I** qRT-PCR-assayed transcript levels of mitochondria-related genes (*TFAM*, *POLG*, *POLG2*, *SIRT1*, *PPARGC1A*, *CPT1A*, and *CPT1B*) in the indicated groups ($n = 3$ per group). **J** Representative images and (**K**) fluorescence intensity of ER-Tracker-stained oocytes in the indicated groups ($n = 118$ per group). Bar = 100 μm. **L** Representative images of endoplasmic reticulum (ER) distribution in oocytes and (**M**) the proportions of oocytes with abnormal ER distribution in the indicated groups ($n = 3$ per group). Bar = 50 μm. **N** Representative images and (**O**) fluorescence intensity of Fluo-3-stained oocytes in the indicated groups ($n = 50$ per group). Bar = 100 μm. **P** Representative images and (**Q**) fluorescence intensity of Rhod-2-stained oocytes in the indicated groups ($n = 80$ per group). Bar = 100 μm. **R** qRT-PCR-assayed transcript levels of ER stress-related genes (*HSPA5*, *ERN1*, *ATF6*, *DDIT3*, and *ATF4*) in the indicated groups ($n = 3$ per group). **S** Ratios of qRT-PCR-assayed transcript levels of spliced/unspliced *XBP1* genes in the indicated groups ($n = 3$ per group). Data are derived from at least three independent experiments, and different superscripts indicate significant differences ($P < 0.05$). Con, control; RO, 10 μM RO4929097

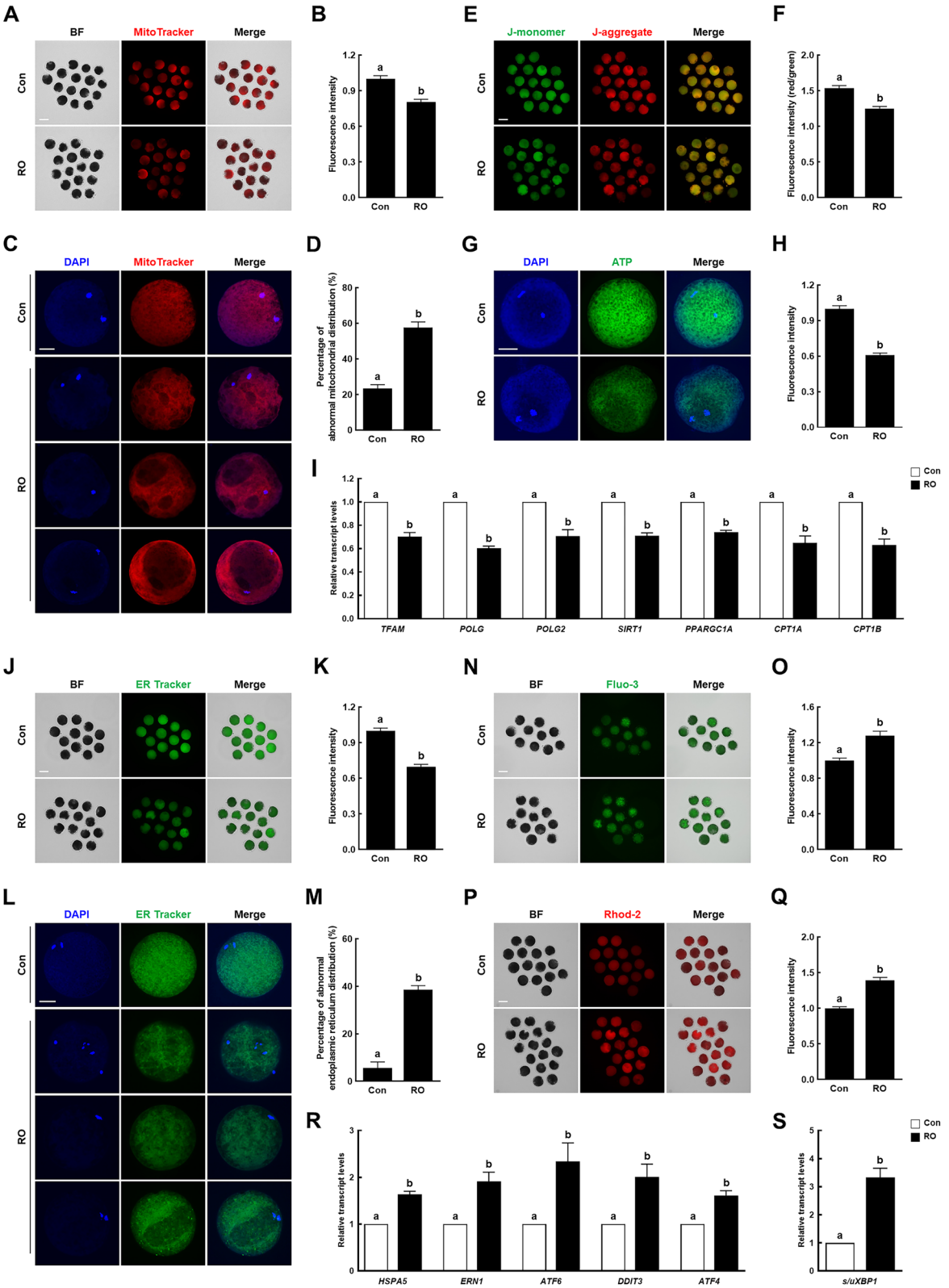

Fig. 5 (See legend on previous page.)

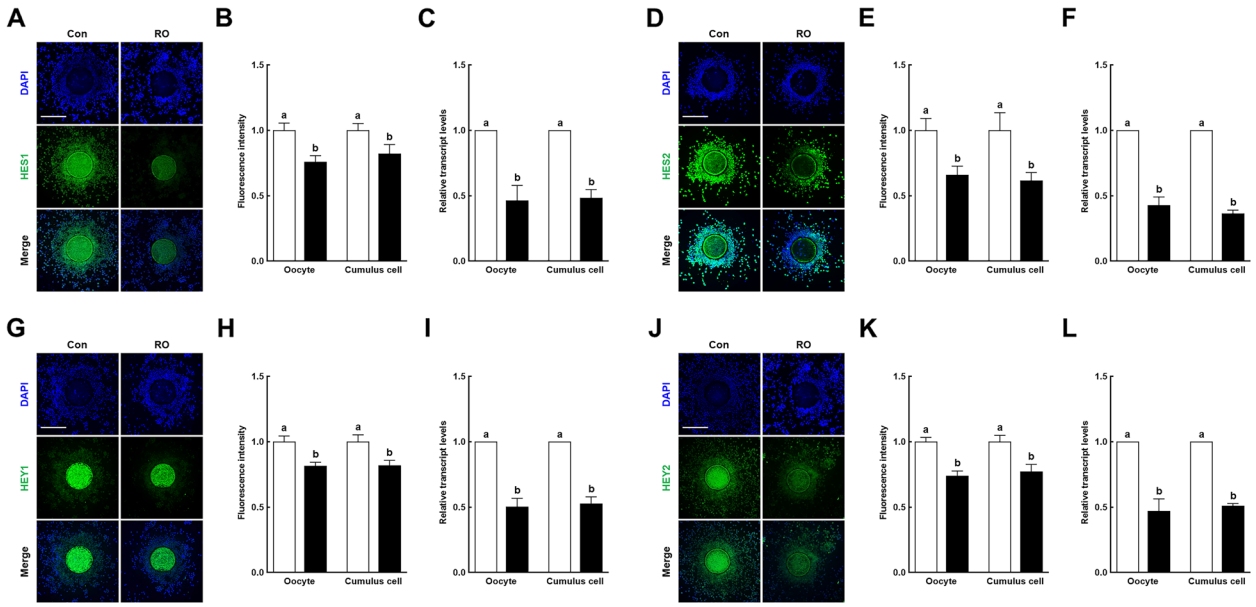

Fig. 6 Effects of Notch signaling inhibition on downstream targets in porcine cumulus–oocyte complexes. **A** Representative images and (**B**) fluorescence intensity of HES1 immunocytochemical staining in cumulus–oocyte complexes (COCs) in the indicated groups ($n = 30$ per group). Bar = 200 µm. **C** qRT-PCR-assayed transcript levels of the *HES1* gene in the indicated groups ($n = 3$ per group). **D** Representative images and (**E**) fluorescence intensity of HES2 immunocytochemical staining in COCs in the indicated groups ($n = 21$ per group). Bar = 200 µm. **F** qRT-PCR-assayed transcript levels of the *HES2* gene in the indicated groups ($n = 3$ per group). **G** Representative images and (**H**) fluorescence intensity of HEY1 immunocytochemical staining in COCs in the indicated groups ($n = 27$ per group). Bar = 200 µm. **I** qRT-PCR-assayed transcript levels of the *HEY1* gene in the indicated groups ($n = 3$ per group). **J** Representative images and (**K**) fluorescence intensity of HEY2 immunocytochemical staining in COCs in the indicated groups ($n = 30$ per group). Bar = 200 µm. **L** qRT-PCR-assayed transcript levels of the *HEY2* gene in the indicated groups ($n = 3$ per group). Data are derived from at least three independent experiments, and different superscripts indicate significant differences ($P < 0.05$). Con, control; RO, 10 µM RO4929097

systems. These findings suggest that the Notch signaling pathway is important for the meiotic maturation of porcine oocytes (Fig. 7).

Mammalian oocyte growth and meiotic maturation occur within the ovarian follicles in vivo [17] and are influenced by follicular somatic cell compartments, such as the granulosa and cumulus cells surrounding the oocyte [18]. Considering this physiological environment of oocyte maturation, several classical signaling pathways involved in ovarian follicular development may play a role in the meiotic maturation of mammalian oocytes. For example, the Notch signaling pathway has been reported to be involved in ovarian follicle development and oocyte maturation in mice [16]. Therefore, we hypothesized and investigated the role of this signaling pathway in porcine oocyte maturation. First, to confirm the existence of the Notch signaling pathway during the meiotic maturation of porcine oocytes, the presence of transcripts and proteins related to the Notch signaling pathway was investigated using RT-PCR and immunocytochemical assays. The results showed that the transcripts and proteins of Notch receptors (NOTCH1–4) and ligands (JAG1 and 2 and DLL1, 3, and 4) were continuously expressed in both oocytes and cumulus cells throughout IVM, indicating that the Notch signaling pathway is involved in the meiotic maturation of porcine oocytes.

During oocyte meiotic maturation, the cumulus expansion of COCs [19] and nuclear and cytoplasmic maturation of oocytes [20] are needed to acquire developmental competence. The optimum expansion of cumulus cells is essential for proper oocyte maturation [21], fertilization, and embryo development [22]. Therefore, cumulus cell expansion has been used as a visual indicator of oocyte maturation [23]. Additionally, oocyte nuclear and cytoplasmic maturation can be evaluated by counting the number of mature oocytes with polar body extrusion and examining subsequent embryogenesis, respectively [24]. Therefore, to investigate the role of the Notch signaling pathway during porcine oocyte maturation, the effects of its inhibition by RO on cumulus cell expansion, oocyte nuclear maturation, and subsequent embryo development after parthenogenetic activation were examined. During the entire IVM period, 10 µM RO significantly reduced cumulus cell expansion, decreasing the level of all transcripts (*SHAS2*, *PTGS1*, *PTGS2*, and *TNFAIP6*) related to this process. These results indicate that the

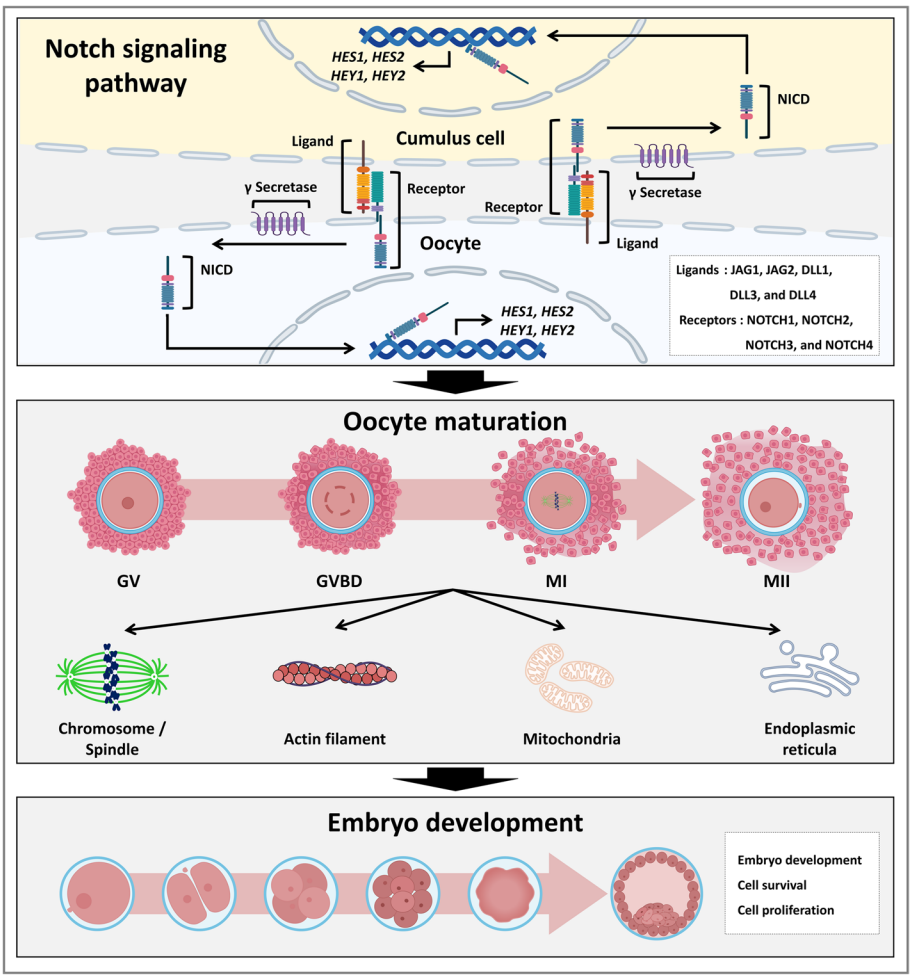

Fig. 7 Graphical overview of the canonical role and potential regulatory mechanisms of the Notch signaling pathway on porcine oocyte maturation. Notch signaling-related transcripts and proteins were continuously detected in oocytes and cumulus cells during meiotic maturation. Notably, the Notch signaling regulates microtubule function, including spindle organization and chromosome segregation, and supports proper cytoplasmic maturation by maintaining homeostasis of the mitochondrial and ER systems in porcine oocytes. These findings provide novel insights into the canonical role and potential regulatory mechanisms of the Notch signaling pathway in porcine oocyte maturation

Notch signaling pathway is required for proper expansion of the cumulus cell layers during oocyte meiotic maturation. With regard to oocyte nuclear maturation, the rate of MII in the 10 μM RO-treated group was markedly decreased together with the downregulated level of proteins and transcripts related to oocyte competence (GDF9 and BMP15) and genes related to mitogen-activated protein kinase (*MOS*) and maturation promoting factor (*CCNB1* and *CDK1*). These results suggest that the nuclear maturation of porcine oocytes is under the control of the Notch signaling pathway during meiotic maturation. With regard to subsequent embryo development, 10 μM RO significantly decreased the rate of blastocyst formation and reduced their total cell number, including those in the inner cell mass and trophectoderm. Furthermore, the transcript levels of developmental potential-related genes (*POU5F1*, *NANOG*, *SOX2*, *CDX2*, *TEAD4*, and *GATA3*) were significantly reduced by 10 μM RO. Additionally, 10 μM RO-treated blastocysts showed a significantly increased percentage of apoptotic cells, with decreased level of *BCL2L1* transcripts. These results suggest that proper oocyte meiotic maturation under the control of the Notch signaling pathway is important for subsequent porcine embryo development.

To comprehensively investigate the effects of Notch inhibition on oocyte nuclear maturation, we analyzed cell cycle progression, spindle assembly, and chromosome alignment in porcine oocytes matured in the presence of 10 μM RO. The inhibitor treatment delayed cell cycle progression and increased the incidence of aneuploidy in

porcine oocytes. Previous studies have shown that precise spindle assembly is critical for spindle organization and accurate chromosome segregation during meiosis, with errors in these processes causing the production of developmentally compromised aneuploid oocytes [25, 26]. As expected, RO treatment resulted in abnormal spindle assembly, including aberrant spindles, misaligned chromosomes, a higher number of lagging chromosomes, and abnormal spindle/chromosome structures in porcine oocytes. These results are consistent with those of a previous study, which showed that disrupted Notch signaling causes abnormal spindle assembly, which leads to failure of complete meiosis and thus impaired meiotic maturation [27]. These observations of abnormal spindle assembly prompted us to further investigate the role of Notch signaling in the regulation of microtubule stability. RO treatment significantly reduced the level of acetylated tubulin, which is important for maintaining the structure and stability of microtubules [28]. Collectively, these results suggest that Notch signaling plays a crucial role in microtubule stability and function, including spindle organization and chromosome rearrangement, during oocyte meiotic maturation.

Organelle and chromosome rearrangements within the oocyte are important for successful meiotic maturation by ensuring simultaneous maturation of the cytoplasm and nucleus, which leads to normal fertilization and subsequent embryo development [29]. The microtubule and microfilament dynamics are associated with the rearrangement of organelles such as the mitochondria and ERs, the proper rearrangement and activation of which are important indicators of cytoplasmic maturation [30]. We observed abnormal spindle organization and actin morphology in the RO-treated oocytes. On the basis of these observations, we predict that Notch signaling affects the distribution and function of organelles in the oocyte cytoplasm. Mitochondria provide most of the ATP required to support spindle assembly and chromosome segregation and regulate calcium oscillations during fertilization [31]. During oocyte maturation, mitochondria redistribute from the cortex in the germinal vesicle stage and diffuse until maturation is complete, and their activity gradually increases [32]. RO significantly decreased the mitochondrial content, proportion of normal mitochondrial distribution, mitochondrial membrane potential, and ATP content in porcine oocytes, suggesting that Notch signaling regulates mitochondrial distribution and function during oocyte maturation. Additionally, the ER plays an important role in oocyte metabolic renewal, such as the synthesis, transport, and folding of cytoplasmic proteins and lipid synthesis [33]. The ER also acts as the main storage site for calcium ions, which control the resumption and completion of meiosis, prevention of polyspermy, and accumulation of maternal mRNAs [34]. The RO-treated oocytes had a lower ER content, uneven ER distribution, and elevated mitochondrial and cytoplasmic calcium ion levels, indicating that Notch signaling controls ER distribution and calcium homeostasis during oocyte maturation. Moreover, excessive calcium influx within the oocyte cytoplasm may affect ER function, leading to the accumulation of unfolded or misfolded proteins, which cause ER stress [35]. Severe or prolonged stress can cause redistribution and structural changes in the ERs and interfere with the synthesis and processing of proteins required for meiosis [36]. RO significantly increased the transcript levels of ER stress-related genes and the ratio of spliced/unspliced *XBP1*, indicating that these inhibitor-treated oocytes were under ER stress. Collectively, these results suggest that Notch signaling supports proper cytoplasmic maturation through regulation of the mitochondrial and ER systems during porcine oocyte maturation, contributing to subsequent embryo development. Finally, the substantial decreases in HES1, HES2, HEY1, and HEY2 transcripts and proteins in RO-treated COCs were further proof that the canonical Notch signaling pathway is essential for the meiotic maturation of porcine oocytes.

In conclusion, this study is the first to investigate the importance of the Notch signaling pathway in mammalian oocyte maturation. We concluded that Notch signaling plays an important role in porcine oocyte meiotic progression by regulating microtubule function, including spindle organization and chromosome segregation, and supports proper oocyte cytoplasmic maturation by maintaining homeostasis of the mitochondrial and ER systems. These findings provide novel insights into the canonical role and potential regulatory mechanisms of the Notch signaling pathway in female reproductive biology. However, because oocyte maturation in vivo is regulated by multiple factors, including hormonal signals, interactions between oocytes and somatic cells, and other signaling pathways, the role of Notch signaling in oocyte maturation revealed in this study may differ from that in vivo.

Abbreviations

NOTCH	Notch receptor
JAG	Jagged
DLL	Delta-like canonical Notch ligand
NICD	Notch intracellular domain
COCs	Cumulus–oocyte complexes
RO	RO4929097
IVM	In vitro maturation
ER	Endoplasmic reticulum
MI	Metaphase I
MII	Metaphase II
CDX2	Caudal type homeobox 2
PMSG	Pregnant mare serum gonadotropin
hCG	Human chorionic gonadotropin
DPBS	Dulbecco's phosphate-buffered saline

BSA	Bovine serum albumin
DAPI	4′,6-Diamidino-2-phenylindole
TUNEL	Terminal deoxynucleotidyl transferase-mediated dUTP-digoxygenin nick end-labeling
RT-PCR	Reverse transcription polymerase chain reaction

Supplementary Information

The online version contains supplementary material available at https://doi.org/10.1186/s12964-024-01996-x.

Supplementary Material 1.

Acknowledgements
Not applicable.

Authors' contributions
P.S.J. and H.G.K. carried out the Conceptualization, Investigation, Formal analysis, Validation, Visualization, Data curation, and Writing – original draft. D.C., S.B.J., M.J.K., and B.S.S. carried out the Investigation and Writing – review & editing. B.W.S. carried out the Supervision, Validation, Resources, and Writing – review & editing. S.L. carried out the Supervision, Validation, Project administration, Funding acquisition, Writing – original draft, review, & editing. All authors have read and agreed to the published version of the manuscript.

Funding
This work was supported by the National Research Foundation of Korea (NRF) grant funded by the Korea government (MSIT) (No. 2022R1F1A1067360 and No. 00210823) and the Korea Research Institute of Bioscience and Biotechnology (KRIBB) Research Initiative Program (KGM4252432).

Data availability
No datasets were generated or analysed during the current study.

Declarations

Ethics approval and consent to participate
Animal experiments were approved and reviewed by the Korea Research Institute of Bioscience and Biotechnology (KRIBB) Institutional Animal Care and Use Committee (approval no. KRIBB-AEC-21107, date 03.24.2021) and all studies were conducted in accordance with the Basel Declaration.

Consent for publication
We also confirm that all the listed authors have participated actively in the study, and have seen and approved the submitted manuscript.

Competing interests
The authors declare no competing interests.

Author details
[1]Futuristic Animal Resource and Research Center, Korea Research Institute of Bioscience and Biotechnology, Cheongju 28116, Republic of Korea. [2]Laboratory of Theriogenology, College of Veterinary Medicine, Chungnam National University, Daejeon 34134, Republic of Korea. [3]Department of Functional Genomics, University of Science and Technology, Daejeon 34113, Republic of Korea.

Received: 25 October 2024 Accepted: 12 December 2024
Published online: 02 January 2025

References

1. Rimon-Dahari N, Yerushalmi-Heinemann L, Alyagor L, Dekel N. Ovarian Folliculogenesis. Results Probl Cell Differ. 2016;58:167–90.
2. Richards JS, Pangas SA. The ovary: basic biology and clinical implications. J Clin Invest. 2010;120(4):963–72.
3. Li L, Shi X, Shi Y, Wang Z. The Signaling pathways involved in ovarian follicle development. Front Physiol. 2021;12:730196.
4. Eppig JJ. Reproduction: Oocytes call, granulosa cells connect. Curr Biol. 2018;28(8):R354–6.
5. Perrimon N, Pitsouli C, Shilo BZ. Signaling mechanisms controlling cell fate and embryonic patterning. Cold Spring Harb Perspect Biol. 2012;4(8):a005975.
6. Akil A, Gutierrez-Garcia AK, Guenter R, Rose JB, Beck AW, Chen H, et al. Notch signaling in vascular endothelial cells, angiogenesis, and tumor progression: an update and prospective. Front Cell Dev Biol. 2021;9:642352.
7. Stupnikov MR, Yang Y, Mori M, Lu J, Cardoso WV. Jagged and Delta-like ligands control distinct events during airway progenitor cell differentiation. Elife. 2019;8:e50487
8. Zhou B, Lin W, Long Y, Yang Y, Zhang H, Wu K, et al. Notch signaling pathway: architecture, disease, and therapeutics. Signal Transduct Target Ther. 2022;7(1):95.
9. Papadopoulou AA, Fluhrer R. Signaling functions of intramembrane aspartyl-proteases. Front Cardiovasc Med. 2020;7:591787.
10. Feng YM, Liang GJ, Pan B, Qin XS, Zhang XF, Chen CL, et al. Notch pathway regulates female germ cell meiosis progression and early oogenesis events in fetal mouse. Cell Cycle. 2014;13(5):782–91.
11. Andersen P, Uosaki H, Shenje LT, Kwon C. Non-canonical Notch signaling: emerging role and mechanism. Trends Cell Biol. 2012;22(5):257–65.
12. Li S, Shi Y, Dang Y, Luo L, Hu B, Wang S, et al. NOTCH signaling pathway is required for bovine early embryonic developmentdagger. Biol Reprod. 2021;105(2):332–44.
13. Chang CH, Liu YT, Weng SC, Chen IY, Tsao PN, Shiao SH. The non-canonical Notch signaling is essential for the control of fertility in Aedes aegypti. PLoS Negl Trop Dis. 2018;12(3):e0006307.
14. Alfred V, Vaccari T. Mechanisms of non-canonical signaling in health and disease: diversity to take therapy up a notch? Adv Exp Med Biol. 2018;1066:187–204.
15. Zhang CP, Yang JL, Zhang J, Li L, Huang L, Ji SY, et al. Notch signaling is involved in ovarian follicle development by regulating granulosa cell proliferation. Endocrinology. 2011;152(6):2437–47.
16. Manosalva I, Gonzalez A, Kageyama R. Hes1 in the somatic cells of the murine ovary is necessary for oocyte survival and maturation. Dev Biol. 2013;375(2):140–51.
17. Clarke HJ. Regulation of germ cell development by intercellular signaling in the mammalian ovarian follicle. Wiley Interdiscip Rev Dev Biol. 2018;7(1):e294.
18. Da Broi MG, Giorgi VSI, Wang F, Keefe DL, Albertini D, Navarro PA. Influence of follicular fluid and cumulus cells on oocyte quality: clinical implications. J Assist Reprod Genet. 2018;35(5):735–51.
19. Nevoral J, Orsák M, Klein P, Petr J, Dvořáková M, Weingartová I, et al. Cumulus cell expansion, its role in oocyte biology and perspectives of measurement: a review. Sci Agric Bohem. 2015;45:212–25.
20. Rybska M, Knap S, Jankowski M, Jeseta M, Bukowska D, Antosik P, et al. Cytoplasmic and nuclear maturation of oocytes in mammals–living in the shadow of cells developmental capability. Med J Cell Biol. 2018;6(1):13–7.
21. Moulavi F, Hosseini SM. Diverse patterns of cumulus cell expansion during in vitro maturation reveal heterogeneous cellular and molecular features of oocyte competence in dromedary camel. Theriogenology. 2018;119:259–67.
22. Fair T, Lonergan P. The oocyte: the key player in the success of assisted reproduction technologies. Reprod Fertil Dev. 2023;36(2):133–48.
23. Garcia Barros R, Lodde V, Franciosi F, Luciano AM. A refined culture system of oocytes from early antral follicles promotes oocyte maturation and embryo development in cattle. Reproduction. 2023;165(2):221–33.
24. Yang HJ, Lee S, Sim BW, Jeong PS, Choi SA, Park YH, et al. Transient meiotic arrest maintained by DON (6-diazo-5-oxo-l-norleucine) enhances nuclear/cytoplasmic maturation of porcine oocytes. Reproduction. 2019;158(6):543–54.
25. Kincade JN, Hlavacek A, Akera T, Balboula AZ. Initial spindle positioning at the oocyte center protects against incorrect kinetochore-microtubule attachment and aneuploidy in mice. Sci Adv. 2023;9(7):eadd7397.
26. Mihajlovic AI, Byers C, Reinholdt L, FitzHarris G. Spindle assembly checkpoint insensitivity allows meiosis-II despite chromosomal defects in aged eggs. EMBO Rep. 2023;24(11):e57227.
27. Vanorny DA, Mayo KE. The role of Notch signaling in the mammalian ovary. Reproduction. 2017;153(6):R187–204.

28. Eshun-Wilson L, Zhang R, Portran D, Nachury MV, Toso DB, Lohr T, et al. Effects of alpha-tubulin acetylation on microtubule structure and stability. Proc Natl Acad Sci U S A. 2019;116(21):10366–71.
29. Adhikari D, Lee IW, Yuen WS, Carroll J. Oocyte mitochondria-key regulators of oocyte function and potential therapeutic targets for improving fertility. Biol Reprod. 2022;106(2):366–77.
30. Mao L, Lou H, Lou Y, Wang N, Jin F. Behaviour of cytoplasmic organelles and cytoskeleton during oocyte maturation. Reprod Biomed Online. 2014;28(3):284–99.
31. Yu Y, Dumollard R, Rossbach A, Lai FA, Swann K. Redistribution of mitochondria leads to bursts of ATP production during spontaneous mouse oocyte maturation. J Cell Physiol. 2010;224(3):672–80.
32. Hao X, Zhao J, Rodriguez-Wallberg KA. Comprehensive atlas of mitochondrial distribution and dynamics during oocyte maturation in mouse models. Biomark Res. 2024;12(1):125.
33. Kang X, Wang J, Yan L. Endoplasmic reticulum in oocytes: spatiotemporal distribution and function. J Assist Reprod Genet. 2023;40(6):1255–63.
34. Chen C, Huang Z, Dong S, Ding M, Li J, Wang M, et al. Calcium signaling in oocyte quality and functionality and its application. Front Endocrinol (Lausanne). 2024;15:1411000.
35. Braakman I, Bulleid NJ. Protein folding and modification in the mammalian endoplasmic reticulum. Annu Rev Biochem. 2011;80:71–99.
36. Pan MH, Wu YK, Liao BY, Zhang H, Li C, Wang JL, et al. Bisphenol A exposure disrupts organelle distribution and functions during mouse oocyte maturation. Front Cell Dev Biol. 2021;9:661155.

Publisher's Note